Structure of *Foot-and-mouth disease virus* serotype $A10_{61}$ alone and complexed with oligosaccharide receptor: receptor conservation in the face of antigenic variation

Elizabeth E. Fry,[1] John W. I. Newman,[2] Stephen Curry,[2,3] Saloua Najjam,[2] Terry Jackson,[2] Wendy Blakemore,[2]† Susan M. Lea,[4] Laura Miller,[2]‡ Alison Burman,[2] Andrew M. Q. King[2] and David I. Stuart[1]

Correspondence
David I. Stuart
dave@strubi.ox.ac.uk

[1]Division of Structural Biology, The Henry Wellcome Building for Genomic Medicine, Roosevelt Drive, Headington, Oxford OX3 7BN, UK

[2]Institute for Animal Health, Ash Road, Pirbright, Woking GU24 0NF, UK

[3]Biophysics Section, The Blackett Laboratory, Imperial College, South Kensington Campus, London SW7 2AZ, UK

[4]Laboratory of Molecular Biophysics, Rex Richards Building, South Parks Road, Oxford OX1 3QU, UK

Foot-and-mouth disease viruses (FMDVs) target epithelial cells via integrin receptors, but can acquire the capacity to bind cell-surface heparan sulphate (or alternative receptors) on passage in cell culture. Vaccine viruses must be propagated in cell culture and, hence, some rationale for the selection of variants in this process is important. Crystal structures are available for type O, A and C viruses and also for a complex of type O strain O_1BFS with heparin. The structure of FMDV $A10_{61}$ (a cell culture-adapted strain) complexed with heparin has now been determined. This virus has an RGSD motif in place of the otherwise conserved RGD integrin-binding motif and the potential to bind heparan sulphate (suggested by sequence analyses). FMDV $A10_{61}$ was closely similar in structure to other serotypes, deviating most in antigenic sites. The VP1 GH loop comprising the integrin-binding motif was disordered. Heparin bound at a similar site and in a similar conformation to that seen in the analogous complex with O_1BFS, although the binding had a lower affinity and was more ionic.

Received 27 October 2004
Accepted 23 March 2005

INTRODUCTION

The seven serotypes of *Foot-and-mouth disease virus* (FMDV) (A, O, C, Asia1, SAT1, SAT2 and SAT3), together with *Equine rhinitis A virus*, constitute the genus *Aphthovirus* of the family *Picornaviridae*. FMDVs are highly contagious, infecting cloven-hoofed animals, and outbreaks of disease have great economic importance. Control and eradication of the virus through vaccination and/or slaughter have not proven satisfactory and a more rigorous understanding of the basis of antigenic variation and receptor utilization may lead to improved vaccines or novel methods of control.

The ~300 Å (30 nm) diameter protein capsid of picornaviruses encloses an infectious, single-stranded RNA genome encoding a single polyprotein, which is cleaved post-translationally by viral proteases to yield the viral structural and non-structural proteins. The mature capsid comprises 60 copies each of four proteins – VP1 (1D), VP2 (1B), VP3 (1C) and VP4 (1A) – arranged in a pseudo $T=3$ icosahedral lattice (Fig. 1a). VP1, VP2 and VP3 are wedge-shaped, eight-stranded β-sandwiches, with strands denoted CHEF and BIDG, and fit together with the CHEF sheet exposed on the capsid surface and BIDG to the interior. The loops connecting the strands at the narrow end of the wedge (BC, HI, DE and FG) are less constrained by structural interactions and tend to mediate host interactions. VP4 and the N termini of VP1 and VP3 are located at the capsid interior.

†Present address: Astex Technology Ltd, 436 Cambridge Science Park, Milton Road, Cambridge CB4 0QA, UK.

‡Present address: Animal Health Research Unit, US Meat Animal Research Center, ARS USDA, PO Box 166, State Spur 18D, Clay Center, NE 68933, USA.

Atomic coordinates have been deposited in the Protein Data Bank under accession codes 1ZBE and 1ZBA.

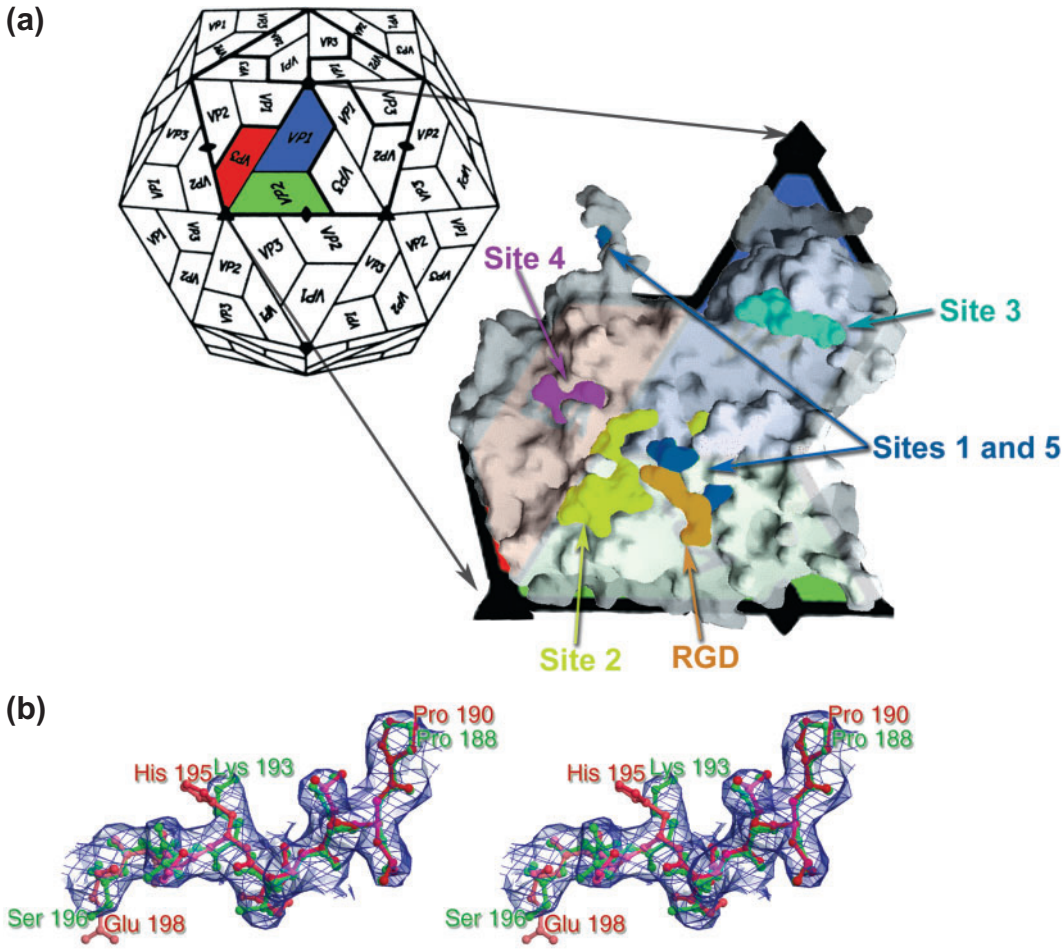

Fig. 1. Structure determination. (a) Schematic depiction of a picornaviral icosahedral capsid, showing the pseudo $T=3$ arrangement of 60 copies of each of the viral proteins VP1–4. An individual subunit (the biological protomer deriving from the uncleaved polyprotein) is coloured as standard: VP1 blue, VP2 green, VP3 red (VP4 is not shown as it is internal). This protomer is enlarged and combined with a surface rendition calculated (GRASP; Nicholls *et al.*, 1991) from the coordinates for reduced FMDV O_1BFS, with residues implicated in antigenic sites colour-coded according to the site classification: sites 1 and 5, blue; site 2, khaki; site 3, cyan; site 4, magenta. The Arg-Gly-Asp motif residues are shown in orange. (b) A $2F_{obs}–F_{calc}$ map corresponding to residues 188–196 of VP1 of $A10_{61}$. Electron density is shown as a blue mesh. $A10_{61}$ residues are drawn as green balls and sticks and structurally superimposed O_1BFS residues as red balls and sticks and labelled in the corresponding colours. The electron density shows clearly that the $A10_{61}$ phases have no residual bias from the O_1BFS model used to produce them. Figures were generated by using a version of MOLSCRIPT (Kraulis, 1991) modified by R. Esnouf (Esnouf, 1997, 1999), and Raster3D (Merritt & Murphy, 1994).

Crystallographic structures are available for viruses representative of the A, O and C serotypes (Acharya *et al.*, 1989; Curry *et al.*, 1996; Lea *et al.*, 1994, 1995). These share on average 86 % sequence identity, with VP1 being the most variable protein. There is an underlying structural similarity between the different antigenic sites of the FMDV serotypes (Baxt *et al.*, 1989; Crowther *et al.*, 1993; Lea *et al.*, 1994; Thomas *et al.*, 1988) (Fig. 1a). In all FMDVs, the exposed, mobile loop that connects the G and H strands of VP1 (the GH loop) is central to both the antigenicity of the virus and integrin-receptor binding [see Jackson *et al.* (2003) and references therein]. The highly exposed C terminus of VP1 has also been implicated in antigenicity and receptor binding (Fox *et al.*, 1989; Strohmaier *et al.*, 1982).

The conserved RGD tripeptide, which recognizes the integrin receptor (Jackson *et al.*, 2000, 2002, 2004; Neff *et al.*, 1998), is located in the VP1 GH loop. It is accessible to antibodies (in contrast to the receptor-attachment sites in some other picornaviruses), which neutralize the virus by blocking receptor attachment (Verdaguer *et al.*, 1995, 1997). The GH loop has been structurally disordered in all the native serotypes studied crystallographically to date (Acharya *et al.*, 1989; Curry *et al.*, 1996; Lea *et al.*, 1994,

1995), implying that it has inherent, functionally important mobility. For type O viruses, the stability of the GH loop is governed by a disulphide bond at its base, and a crystallographic analysis of dithiothreitol (DTT)-reduced O_1BFS (Logan *et al.*, 1993) revealed the internal structure of the loop.

Field viruses are dependent on integrin receptors *in vitro* and probably in the infected animal. However, antibody-complexed virus can enter cells that express the Fc receptor (Mason *et al.*, 1993) and adaptation of FMDV to cell culture can result in the selection of virus variants that have a high affinity for heparan sulphate (HS) (Jackson *et al.*, 1996; Sa-Carvalho *et al.*, 1997). HS-adapted variants retain the ability to use integrins, but can also dispense with their RGD integrin-binding site (Sa-Carvalho *et al.*, 1997). Other, as-yet-unidentified classes of cell-surface molecule are also thought to serve as receptors for FMDV (Baranowski *et al.*, 2000; Zhao *et al.*, 2003).

HSs are negatively charged, randomly sulphated polymers of disaccharide repeats of L-iduronic acid (Idu) and D-glucosamine (GlcN) joined by an $\alpha(1–4)$ linkage (see Fig. 3a). They form the carbohydrate component of HS proteoglycans (HSPGs) and are expressed on the surface of virtually all cell types, either as integral membrane proteins or as components of the extracellular matrix, and can mediate internalization of physiological ligands (Bernfield *et al.*, 1999). HS-adapted viruses are characterized by a small-plaque phenotype, increased virulence and expanded host range for cultured cells (Baranowski *et al.*, 2000; Jackson *et al.*, 1996; Neff *et al.*, 1998; Sa-Carvalho *et al.*, 1997), but are attenuated in animal hosts, presumably due to restricted spread and accelerated clearing *in vivo* (Bernard *et al.*, 2000; Byrnes & Griffin, 2000; Klimstra *et al.*, 1998; Lee & Lobigs, 2002; Mandl *et al.*, 2001; Sa-Carvalho *et al.*, 1997). Thus, the functional importance of FMDV–HS interaction *in vivo* remains unclear.

FMDVs of serotypes O (Jackson *et al.*, 1996), A, C (Baranowski *et al.*, 1998), Asia-1 and SAT-1 (S. Najjam, unpublished data) have been shown to bind HSPGs. Many other viruses have been shown to bind and use HSPGs as receptors (Spillmann, 2001), including other picornaviruses, such as the coxsackievirus B3 Nancy variant (PD) (Zautner *et al.*, 2003), Theiler's virus (Reddi *et al.*, 2004) and clinical isolates of echovirus (Goodfellow *et al.*, 2001) and swine vesicular disease virus (Escribano-Romero *et al.*, 2004).

The ability of type O FMDV to bind HS results from one or two residue changes on the outer capsid surface, which lead to a net gain in positive charge (Sa-Carvalho *et al.*, 1997). In O_1BFS (a tissue culture-adapted variant), residue 56 of VP3 switches from the histidine found in field viruses to an arginine, resulting in a partial loss of antigenicity. This arginine is a key bidentate ligand for heparin (Fry *et al.*, 1999). The ability to adapt to a high-affinity HS-binding phenotype may be a feature that is conserved in all FMDVs and, thus, we were interested to know whether such binding was also structurally conserved, as this could throw light on its possible biological significance. Despite the large number of viruses known to recognize HS, with the exception of the atomic resolution of the O_1BFS complex (Fry *et al.*, 1999), there is little information about the molecular mechanisms of the interaction of non-enveloped icosahedral viruses with HS. In this paper, we have reported the native and oligosaccharide receptor-complex structures for a type A FMDV and compared these with the analogous type O structures.

METHODS

Virus and cells. Cells were cultured and virus stocks were prepared as described previously (Jackson *et al.*, 1996, 1997). FMDV $A10_{61}$ is a tissue culture-adapted variant of subtype A10 Holland, highly passaged in BHK cells from the original 1961 Argentinian isolate.

Infectious-centre assay. Infection of Chinese hamster ovary (CHO) and CHOpgsD-677 cells was quantified by using an infectious-centre assay as described previously (Jackson *et al.*, 2000). The zero time point was determined by using parallel cell monolayers that were exposed to virus for 15 min at 4 °C and then treated as above.

Crystallographic analyses

Native virus-structure determination. Plaque-purified clones were passaged in BHK monolayers and purified by sucrose density-gradient centrifugation. Crystals were obtained by sitting-drop vapour diffusion (Harlos, 1992) from solutions containing 2·5–3·0 % PEG 20K and 2 M NH_4Cl at pH 7·6 (Curry *et al.*, 1992). Of the two crystal forms obtained, those used for the initial structure determination exhibited parallelepiped morphology. Macroseeding produced crystals of $0{\cdot}35 \times 0{\cdot}35 \times 0{\cdot}18$ mm, belonging to space group R3 ($a = 295{\cdot}9$ Å, $\beta = 62{\cdot}3°$). The crystallographic asymmetric unit contained one-third of a virion lying on the threefold axis. Crystals were mounted at Pirbright in quartz capillary tubes and exposed to X-radiation at the SRS Daresbury, station 9·6, $\lambda = 0{\cdot}89$ Å, at approximately 290 K. Data for the initial structure determination were recorded on photographic film (CEA Reflex 25), with 0·5° oscillation per exposure. Typically, two consecutive exposures were obtained per crystal. The dataset comprised 60 filmpacks, digitized (50×50 μm raster) on an Optronics P-1000 microdensitometer. The processing protocol was similar to that described previously (Fry *et al.*, 1993), using MOSCO9 and CCP4 programs (Collaborative Computational Project, Number 4, 1994). Partially recorded reflections (>70 %) were scaled up (statistics are given in Table 1).

In the diffraction data, *32* symmetry was apparent at low resolution. Hence, a 20-mer search model was made from the FMDV O_1BFS coordinates (1BBT; Berman *et al.*, 2000), orientated with a twofold axis along X and threefold along Z. Rigid-body refinement (XPLOR; Brunger, 1992) using data from 8 to 3 Å (final *R* factor, 32·7 %) revealed that the particle twofold axes were misaligned from rhombohedral (*R32*) twofold axes by a 0·9° rotation about the crystallographic threefold, hence the pseudo-*R32* nature of the diffraction. An iterative rigid-body search made with XPLOR (Brunger, 1992) using 50 to 3 Å data defined the cell dimensions as $a = 295{\cdot}9$ Å, $\alpha = 62{\cdot}3°$. Positional refinement yielded improved phase estimates, which were further improved by a cycle of 20-fold non-crystallographic symmetry averaging using GAP (D. I. Stuart & J. Grimes, unpublished data). The averaged $2|F_o| - |F_c|$ map was extremely clear, enabling the correct $A10_{61}$ sequence (Boothroyd *et al.*, 1982) and structural changes to be

Table 1. X-ray data collection and structure-refinement statistics

	Native	Complex
Data collection and processing		
Space group	R3	R3
Unit cell (hexagonal)	$a=b=306{\cdot}2$ Å, $c=712{\cdot}8$ Å, $\alpha=\beta=90^\circ$, $\gamma=120^\circ$	$a=b=307$ Å, $c=715$ Å, $\alpha=\beta=90^\circ$, $\gamma=120^\circ$
Wavelength (Å)	0·89	0·87
D_{min} (Å)	3·0	2·0
No. crystals	30–40	~15
No. images	60	80
Rotation per image (°)	0·5	0·4/0·3
No. unique reflections	289 979	457 381
R merge (%)*	17·5	13·5
Completeness (to D_{min} Å) (%)†	58·1†	26·6
Refinement		
Data range (Å)	55–3	30–2
No. unique reflections	289 692	452 651
Final statistics:		
R factor (%)‡	21·4	18·3
Protein atoms	6413	6413
Solvent	NA	450
Non-protein atoms	NA	55
R.m.s.d. bond lengths (Å)§	0·01	0·01
R.m.s.d. angles (°)§	1·8	1·7
R.m.s.d. B main chain (Å^2)	2·8	4·7
R.m.s.d. B side chain (Å^2)	3·9	8·0
Mean *B* factor (Å^2)	23·7	31·4

*$R=100\times\Sigma_h\Sigma_j|I_{h,\ merged}-I_{h,\ j}|/\Sigma_h N|I_{h,\ merged}|$, where $j=1, ..., N$ for N datasets.
†Completeness of the highest-resolution shell (3·11–3·0 Å) was 46 %.
‡$R=100\times\Sigma_h||F_{h,\ obs}|-|F_{h,\ calc}||/\Sigma_h\ |F_{h,\ obs}|$.
§R.m.s.d. from ideal bond lengths or bond angles.

incorporated easily by using FRODO (Jones, 1985). Iterative manual rebuilding and XPLOR refinement (Brunger, 1992) with strict non-crystallographic symmetry (NCS) yielded the final model (Table 1).

Complex structure determination. Crystals could not be grown reliably by using the procedure described above; however, sitting-drop vapour diffusion with either 11–13 % ammonium sulphate or 8–10 % ammonium tartrate as precipitant in 100 mM phosphate buffer, pH 7·6, with 3 mM azide produced similar crystals. These were soaked in 6 kDa porcine heparin (sodium salt; Sigma-Aldrich) at a concentration of 25 mg ml^{-1} for 2 h before mounting in quartz capillaries. Heparin binding could not be detected until the mother liquor was exchanged, to avoid solvent competition for sulphate-binding sites, by stepwise transfer into 10 % PEG 1000, 100 mM phosphate buffer, pH 7·6, and soaked with 6 kDa heparin at a concentration of 25 mg ml^{-1} in this buffer. Diffraction images were collected at room temperature as 0·4° oscillations on a 30 cm imaging plate (MarResearch) at the SRS Daresbury, station 9·6, $\lambda=0{\cdot}87$ Å (Table 1) and processed by using DENZO and SCALEPACK (Otwinoski, 1993). The data were scaled to those for the native virus and combined with phases from the latter for the calculation of difference electron-density maps $|F_{o(soak)}-F_{o(native)}|$. Also, a 2·0 Å resolution omit map $|F_{o(soak)}-F_{c(native)}|$ and $|2F_{o(soak)}-F_{c(native)}|$ map were calculated. These maps were 20-fold-averaged by using GAP (D. I. Stuart & J. Grimes, unpublished data). The electron density was commensurate with three sugar rings with possibly more than one conformation, made unclear by the low occupancy and presumed flexibility. The predominant conformation was built by using, as a starting model, the O_1BFS complex coordinates at a resolution of 1·9 Å (Protein Data Bank code 1QQP). Having verified that there were no significant differences between the NCS-related copies, the model was refined by iterative positional and *B*-factor refinement (XPLOR; Brunger, 1992), using NCS constraints and appropriate stereochemical parameters for heparin (Faham *et al.*, 1996) with the heparin at half occupancy (Table 1).

Surface plasmon resonance (SPR). SPR (Biacore X) was used to measure the binding of free O_1BFS and $A10_{61}$, diluted in different salt concentrations, to immobilized 6 kDa heparin (porcine heparin; Sigma). For this, biotin-labelled heparin was coupled to an SA chip that was derivatized by streptavidin. The same amount of O_1BFS or $A10_{61}$ (40 μg ml^{-1}) was injected at a flow rate of 40 μl min^{-1} at 25 °C.

RESULTS

The electron-density map of the native virus at 3·0 Å resolution clearly differentiated residues that differed between $A10_{61}$ and O_1BFS (Fig. 1b). The model built into this map comprised residues 1–137 and 155–208 of VP1, 12–218 of VP2, 1–221 of VP3 and 15–39 and 62–85 of VP4

(residues 138–154 and 209–212 of VP1, 1–11 of VP2, 1–14 and 40–61 of VP4 are too flexible to be modelled reliably). The final *R* factor for the model was 21·4 %, and 87 % of the residues lay in the most favoured region of the Ramachandran plot, with none in disallowed regions. The structure of the $A10_{61}$–heparin complex at 2 Å resolution showed no noteworthy differences in the capsid structure compared with the uncomplexed virus.

The structure of FMDV $A10_{61}$ was closely similar to that of types O [root mean square deviation (r.m.s.d.) 0·6 $Å^2$; Acharya *et al.*, 1989], C (r.m.s.d. 0·9 $Å^2$; Lea *et al.*, 1994) and another type A virus, A22 Iraq (r.m.s.d. 0·6 $Å^2$) (Curry *et al.*, 1996) (Fig. 2). Variation in the exposed loops and termini accounted for the majority of structural differences between the viruses. The C_α positions within the loops varied by as much as 6 Å between the serotypes and, in some cases, loops adopted a different conformation, e.g. the VP3 GH loop. This level of structural similarity has been observed in other serotype comparisons between polioviruses types 1 and 3 (Filman *et al.*, 1989) and rhinoviruses types 1A and 14 (Kim *et al.*, 1989).

Antigenic surface

Antigenic sites in picornaviruses have been identified from the locations of amino acid substitutions conferring resistance to neutralizing mAbs (MAR substitutions). Although this method identifies only a subset of antibody-contact residues, it has established a correlation between antigenicity and the most accessible surface loops. Thus, the immunodominance of VP1 (and in particular the GH loop of this protein) is attributable to it being the most surface-accessible capsid protein. The antigenicities of type A and C

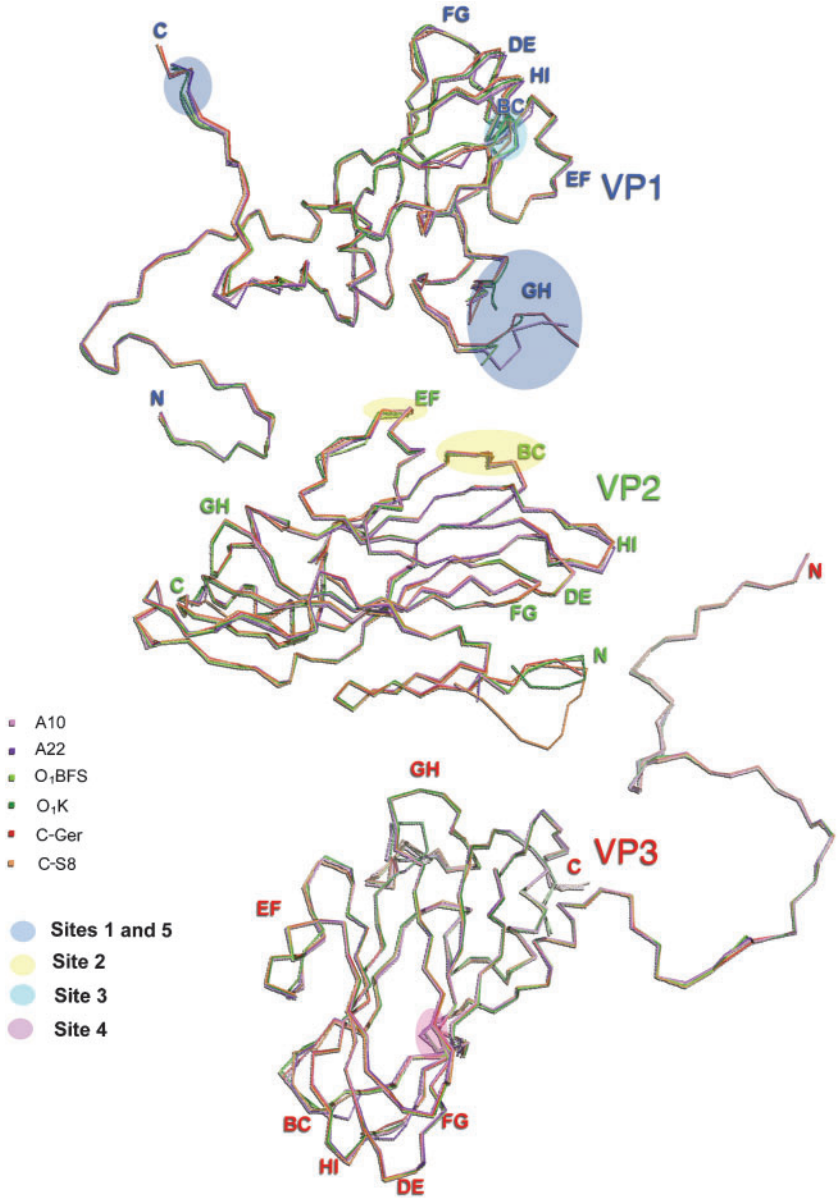

Fig. 2. Structural comparison of European serotypes. The relatively small main-chain deviations between European subtypes are shown by superimposing proteins VP1, VP2 and VP3 for the available structures (Structural Homology Program; Stuart *et al.*, 1979). Each protein is drawn as a worm and colour-coded such that $A10_{61}$ is pink, A22 purple, O_1BFS lime green, O_1K dark green, C-Ger red and C-S8 orange. Surface-oriented loops are labelled and antigenic-site regions are colour-coded as in Fig. 1(a).

viruses broadly resemble that of type O; thus, we will principally use the definitions of type O antigenic sites by Kitson *et al.* (1990) as the basis for comparing the antigenic surfaces of representative members of the A, O and C serotypes. A superimposition of the individual proteins can be seen in Fig. 2.

VP1 GH loop [MAR substitutions at residues 144, 148 and 154 (site 1) and residue 149 (site 5)]. In $A10_{61}$, this loop was disordered between residues 138 and 154, corresponding closely to the native structures for C-S8 (missing residues 133–156) and A22 (missing residues 137–155), none of which have the destabilizing disulphide bridge peculiar to O_1BFS. There was some evidence for variation in the orientation of the residues leading into and out of the loop, which may be serotype-specific. The observed conformation of the adjacent GH loop of VP3 (which is directly attributable to movement in the VP1 GH loop; Logan *et al.*, 1993) did not seem to be serotype-specific and is possibly not antigenically relevant; two discrete conformations are seen, one in $A10_{61}$, O_1BFS, C-S8 and C-Ger and the other in DTT-treated O_1BFS (Logan *et al.*, 1993), A22 and O_1K (a minor population exhibits the alternative conformation in all strains).

C terminus of VP1 [MAR substitution at residue 208 (site 1)]. In overall disposition, there was a close correspondence between the C termini of VP1 in all serotypes, with a slight variation in the extent of disorder of the terminal three residues. The A serotype viruses had an additional glutamine residue inserted at position 197 in $A10_{61}$ and at 198 in A22, which was highly exposed and resulted in a small deviation (3 Å) in the main chain relative to the other serotypes. In $A10_{61}$, this side chain approached the VP3 β-B 'knob' (site 4) and the intervening residues Lys-843 and Arg-563, which participated in heparin binding.

BC loop of VP2 [MAR substitutions at residues 70–73, 75 and 77 (site 2)]. This loop (residues 70–76) was just long enough to span the distance between the ends of β-strands B and C and structural differences between the serotypes were confined to substituted side chains, despite proline substitutions at residues 71 and 74 of $A10_{61}$.

EF loop of VP2 [MAR substitutions at residues 131 and 134 (site 2)]. There was little main-chain variation in this loop, comprising residues 130–137 of VP2 (maximum deviation between O_1K and O_1BFS, 2 Å at residue 131). The Cys-130 that tethers residue 134 of VP1 in type O viruses is replaced by a lysine in type A viruses, which appears to stabilize the loop by interacting with Glu-136 of VP2. In the serotype C viruses, there is either a glycine or an aspartic acid at position 130. A stabilizing interaction is conserved between a large hydrophobic residue at 129 [Trp (type A), Met (type C), Leu (type O)] and the adjacent strand C.

BC loop of VP1 [MAR substitutions at residues 43–45 and 48 (site 3)]. The differences in main-chain structure of the VP1 loops approaching the fivefold axes between the different serotypes were relatively small, but there was a concerted shift in their position between the A and C serotypes, with the O viruses being intermediate. The greatest differences occurred between the BC loops (residues 43–47), the longest and most exposed loop, which also has the greatest sequence variation. Mutations within this loop can perturb the stability of the immunodominant VP1 GH loop (Parry *et al.*, 1990). The main-chain conformation of the BC loop was clearly serotype-characteristic, making it an antigenic-signature structure. Overall, the O and C serotype BC loops bore more similarity to each other than to the A serotype BC loop (the greatest deviation was 3·8 Å at $A10_{61}$ residue 44). All three serotypes maintained a hydrophobic residue at the centre of the loop, which is possibly required for virion stability (Leu-45 in A22 and $A10_{61}$, Pro-44 in O_1BFS and O_1K and Val-44 in C-S8 and C-Ger). The two proline substitutions within the VP1 BC loop (e.g. Pro-44 in O_1K and O_1BFS and Pro-47 in $A10_{61}$ and A22) both appeared to cause deviations relative to the other serotypes.

β-B 'knob' of VP3 [MAR substitutions at residues 56 and 58 (site 4)]. In the β-B 'knob' region (residues 55–62), the A and O viruses agreed closely in terms of structure. Deletion of the residue corresponding to Asp-59 ($A10_{61}$) in the type C viruses resulted in a main-chain displacement of approximately 3 Å.

Refolding of the adjacent VP3 BC loop. The BC loop of VP3 (residues 66–72) was located in the vicinity of the icosahedral threefold axis and adopted two predominant conformations. In $A10_{61}$, O_1BFS, O_1K and C-Ger, this loop was hinged upward, whilst in A22 (seen at low occupancy in $A10_{61}$) and C-S8, the loop packed closely against the VP3 HI loop underneath. This structural change was not serotype-specific and appeared to be facilitated by peptide flipping. The conformation adopted in the different viruses appeared to be governed largely by a single amino acid substitution. In A22 and C-S8, a glutamine at residue 71 made two H-bonds with the side chain of Glu-138 (a conserved residue) on the adjacent VP3 EF loop. In $A10_{61}$ and O_1BFS, a threonine and an aspartic acid, respectively, occupied this position. The side chains of these residues were too short to make these H-bonds; instead the BC loop was rearranged to allow Arg-72 to H-bond to Glu-138. Thus, conservation of a structural interaction appeared to generate conformational variation.

EF loop of VP3. The conformation of this loop in the type A viruses differed from that in the type O and C viruses. Thr-132 appeared to be a type A-specific insertion, which displaced Glu-131 outward towards the VP1 GH loop. At either end of the loop, there were up to two proline residues (e.g. 127, 133 and 134 in $A10_{61}$; also 128

in A22). Substitutions at these residues in other serotypes did not affect the loop conformation.

Receptor binding

Receptor activity of HS. Infections by FMDV $A10_{61}$ in wild-type CHO cells and the derivative cell line psgD-677, which specifically lacks HS (Esko *et al.*, 1987), were compared by using an infectious-centre assay. The inability of psgD-677 cells to support plaque formation is caused by a defect in virus uptake, which is directly attributable to the absence of HS (Jackson *et al.*, 1996). Fig. 3(b) shows that HS-deficient cells are refractory to infection by $A10_{61}$, whereas the wild-type CHO cells were much more infectable. Infection was blocked completely by 6 kDa heparin at a concentration of 0·5 mg ml^{-1} (data not shown). These data showed that the $A10_{61}$ virus uses HSPG as the receptor on CHO cells and, hence, HS is an abundant ligand for FMDV $A10_{61}$.

Crystallographic analysis. In the analysis of glycosaminoglycan binding to O_1BFS (Fry *et al.*, 1999), a common set of sulphated sugars bound in similarly occupied conformations for two different-molecular-mass species of heparin and HS. Thus, despite heterogeneity in the ligand, the virus selects the appropriate motif. As the highest-resolution data were available for 6 kDa heparin, the same-molecular-mass heparin was chosen for soaking into the $A10_{61}$ crystals (corresponding to a linear chain of approximately 10 disaccharide units). From electrostatic calculations, we predicted that $A10_{61}$ probably binds HS at a similar position on the surface of the virion to O_1BFS (Fry *et al.*, 1999) (Fig. 3a and c), the corresponding region of positive charge being more significant for $A10_{61}$. Difference maps at 3 Å resolution were calculated ($F_{o(soak)}-F_{o(native)}$), which clearly showed the presence of bound sugar. Further maps ($F_{o(soak)}-F_c$) at a resolution of 2·0 Å showed a fully sulphated motif binding with position, orientation and conformation similar to those seen for O_1BFS at 1·9 Å resolution (Fry *et al.*, 1999) (Fig. 3d). However, (in the $A10_{61}$ structure) of the five sugar rings visualized in O_1BFS, there was no obvious electron density for the terminal Idu-1 ring and incomplete density for the Idu-5 ring in $A10_{61}$ (Fig. 3d). The sugar density was no more than 50 % occupied (compared with the protein) and somewhat blurred, suggesting conformational heterogeneity (as observed for O_1BFS), particularly for GlcN-2. The predominant conformation was modelled and the complex was refined at half occupancy, maintaining strict NCS constraints. The final *R* factor was 18·3 % with 0·01 Å r.m.s.d. (bonds).

Heparin-receptor conformation. In O_1BFS, the most tightly bound heparin residues were GlcN-2, Idu-3 and GlcN-4 and, for $A10_{61}$, these were the only ones for which there was clear electron density (Fig. 3d). The GlcN rings adopt the energetically favourable $^4C_1$ or $^1C_4$ chair conformations. GlcN-4 provides the key attachment points to the virus for the extended chain of sugar residues, whilst GlcN-2 is only stabilized by water interactions and shows conformational heterogeneity. The central Idu ring exists in the skew boat ^2S_O conformation. Heparin makes ionic interactions with the protein via sulphates GlcN-4-2-*N*-SO_3, GlcN-4-6-*O*-SO_3 and Idu-3-2-*N*-SO_3, which are closely conserved in position between the A and O serotype complexes. Overall, the ring conformations were similar between the A and O complexes, but differences in ligand interactions gave rise to more flexibility in the central Idu residue in O and more flexibility in ring 2 in A (mean *B* factors: GlcN-4 45, Idu-3 64, GlcN-2 88). Superimpositions of the central trisaccharide from the A and O serotype complexes gave an r.m.s.d. of 1·2 $Å^2$ (CONF 1). Superimpositions of the $A10_{61}$ complex motif with similar central trisaccharide motifs from basic fibroblast growth factor, annexin, a ternary complex with fibroblast growth factor 1 and fibroblast growth factor receptor 2 and NK1 (all coordinates from the Protein Data Bank; Berman *et al.*, 2000), showed strong similarity with the core atoms, superimposing with r.m.s.d. values between 1·2 and 2·0 $Å^2$.

Attachment site. The topology of the heparin-binding site was virtually identical for the type A and O viruses, with a shallow depression at the junction of the three major capsid proteins within the biological protomer, distinct from the integrin-binding site (Fig. 3a). The walls of the depression are formed by strand B1 of VP3 (residues 55–58) and the subsequent loop (residues 58–60), the C terminus of VP1 (residues 195–197) and the αB helix of VP2 (residues 133–138). The base of the depression is formed by a 3_{10} helix (residues 84–88) of VP3 (Fig. 4a). The central trisaccharide occluded ~400 $Å^2$ of solvent-accessible surface on the virus. There were virtually no changes in the protein to accommodate the sugar. The ligands were the basic and polar residues Arg-56 and Asn-88 of VP3, Thr-134 and Arg-135 of VP2 and Lys-193 of VP1, and bridging water molecules were important (Fig. 4b). As for O_1BFS, there was no direct involvement of the VP1 C-terminal residues ^{200}RHKQI^{205} in binding; however, the neighbouring residues His-195 (O_1BFS) (Fig. 4b) and Lys-193 ($A10_{61}$) of VP1 (Fig. 4a) did contact the HS, and the C terminus may stabilize these residues in a suitable position for HS binding.

Two liganding residues were conserved between the type A and O complexes: Arg-56 of VP3 and Arg-135 of VP2 (Fig. 4a and b). The former switches from a histidine to an arginine in type O viruses on adaptation to tissue culture and is a key ligand in both complexes. In the O_1BFS complex, it acts as a bidentate ligand, stabilizing sulphate groups from rings 2 and 4, whereas in the $A10_{61}$ complex, it only interacts with ring 4. Arg-135 makes a hydrophobic interaction in both complexes and appears to polarize Asn-88 of VP3, increasing its affinity for GlcN-4-6-*O*-SO_3. Overall, the protein contacts are more ionic for the $A10_{61}$ than the O_1BFS complex (Fig. 4), principally because a

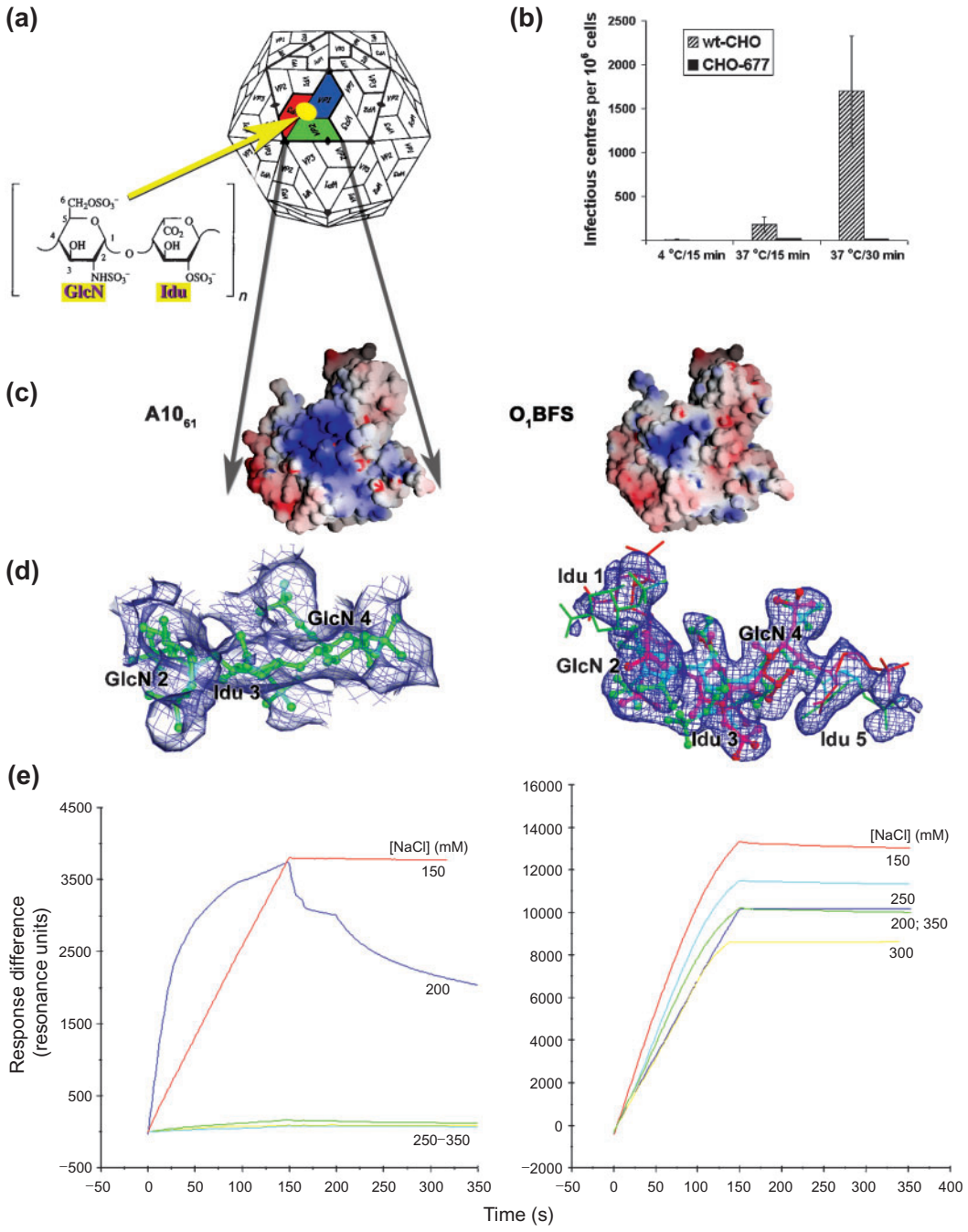

Fig. 3. Heparin-binding analysis. (a) Schematic of a picornaviral capsid (as in Fig. 1a), showing the location of the heparin-binding site within the biological protomer. The inset shows a typical heparin disaccharide containing a total of three sulphate groups: one attached to the 2-hydroxyl group of Idu and two linked to the 2-amino and 6-hydroxyl groups of GlcN. In the non-bound structure, successive disaccharides within heparin are related by a twofold screw operation generated by a rotation angle of ~180° coupled to a translation of 8·0–8·7 Å along the helix axis. (b) Effect of cell-surface HS on the susceptibility to infection with $A10_{61}$. The number of productive infection events at 37 and 4 °C were scored at the indicated times on wt CHO cells (hatched bars) and cells lacking HS (solid bars) by using an infectious-centre assay (see Methods). (c) GRASP (Nicholls *et al.*, 1991) electrostatic, accessible-surface depictions for the biological protomer of $A10_{61}$ (left) and O_1BFS (right). The GH loop is absent in both representations. The scale on which the electrostatic potential was measured was similar for each serotype, with positive charge in blue and negative charge in red. (d) F_o–F_c omit maps for the sugar residues bound to $A10_{61}$ (left) and O_1BFS (right). Electron density is drawn as a blue mesh and the sugar coordinates are depicted as green balls and sticks for $A10_{61}$ and the two conformations bound to O_1BFS in green and red balls and sticks. (e) Analysis of heparin binding to $A10_{61}$ (left) and O_1BFS (right) at various salt concentrations by SPR.

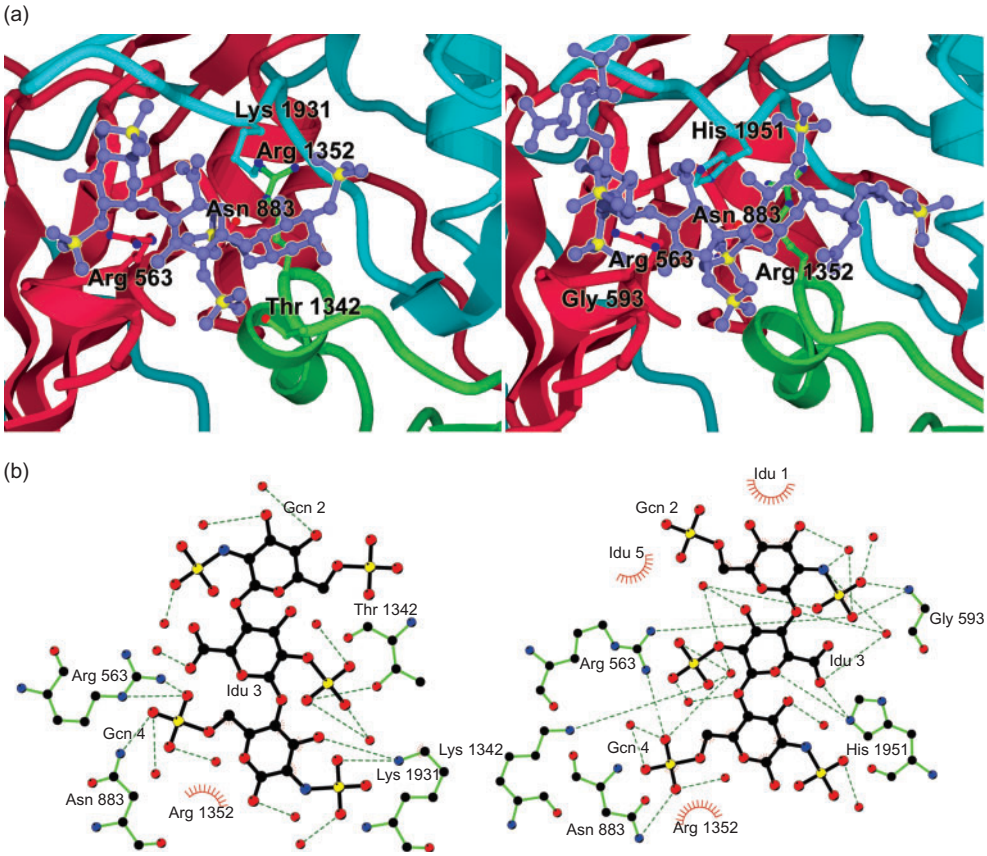

Fig. 4. Heparin-binding site. (a) Ligand-binding site in A10$_{61}$ (left) and O$_1$BFS (right). Viral proteins are depicted as ribbons with standard colour coding. The side chains of ligand residues (labelled) are drawn as balls and sticks in the same colour as the corresponding protein. They are labelled with the residue number and the chain ID as the least significant digit, e.g. 563 is residue 56 of VP3. The sugar residues are depicted as purple balls and sticks, with sulphur atoms in yellow. (b) Sugar–protein interactions depicted by using LIGPLOT (Wallace *et al.*, 1995). A10$_{61}$ is shown (left) and the central three sugars of CONF1 (Fry *et al.*, 1999) bound to O$_1$BFS (right). Only protein side chains that interact directly are shown and these are rearranged to clarify the hydrogen-bonding pattern. Ligand bonds are drawn in purple and non-ligand bonds in brown. Hydrogen bonds are depicted by olive-green, dashed lines. Non-ligand residues involved in hydrophobic contacts are shown as red, fringed semicircles. Water molecules are coloured red.

central, non-ionic contact in the O$_1$BFS complex contributed by His-195 of VP1 is replaced by an ionic interaction of Lys-193 of VP1 in A10$_{61}$. This presumably explains the fact that, whilst for O$_1$BFS, heparin at a concentration of 3 mM was able to displace sulphates present at a concentration of 0·8 M (from the ammonium sulphate mother liquor), for A10$_{61}$, bound sugar was only observed when the ammonium sulphate mother liquor was exchanged for PEG. This was confirmed by SPR analysis (Fig. 3e) comparing heparin binding by O$_1$BFS and A10$_{61}$ under different salt concentrations. Very weak binding between heparin and A10$_{61}$ was observed above 250 mM NaCl, and at 200 mM the A10$_{61}$–heparin complex dissociated rapidly. Thus, A10$_{61}$ has a low affinity for heparin.

DISCUSSION

The A10$_{61}$ virus capsid showed no unexpected deviations from the previously reported FMDV capsid structures. The disorder of the highly immunogenic VP1 GH loop was in line with that of other FMDV capsids and underlines the biological role of its flexibility for immune evasion or induced fit.

A comparison of the capsids of the different viruses revealed no greater overall structural similarity between members of the same serotype than between different serotype structures. This reflects significant switches in loop disposition, possibly arising from movements in adjacent structures that are not serotype-specific and may not be antigenically relevant. However, the regions of the structure assigned as antigenic sites showed greater similarity within serotypes. Structural differentiation between serotypes may be mediated by the conversion of residues to and from conformationally restricted proline residues. However, proline residues do not always lead to conformational changes (e.g. site 2) and, conversely, minimal insertions, deletions and switches in electrostatic

or hydrophobic character can also mediate dramatic changes in antibody recognition.

FMDVs O_1BFS and $A10_{61}$ are both highly passaged viruses, but the O and A serotypes diverged a long time ago, so that they differ in several of the HS-contact residues. Thus, the conservation of a binding site that is predisposed to acquire by mutation a high affinity for HS may be biologically significant. Both the O_1BFS and $A10_{61}$ complexes with heparin share certain characteristics: minimal buried surface area, some shape complementarity, high charge interaction, little change in the binding site on heparin binding, recognition of both *N* and *O* sulpho groups and a tight-binding core trisaccharide [also seen in the polyomavirus–sialic acid complex (Stehle *et al.*, 1994) and the bFGF complex with HS (Faham *et al.*, 1996)], corresponding to one turn of the heparin helix. In both A1061 and O_1BFS, the liganding residues are brought together only by the three-dimensional folding of the protein. Hence there is no correspondence to the HS-binding primary-sequence motifs (Cardin & Weintraub, 1989). The interaction in the $A10_{61}$ complex is more ionic and of a lower affinity than that seen in O_1BFS (Fry *et al.*, 1999), but is nevertheless likely to be highly specific. Despite conferring a clear advantage for growth in cultured cells (HS-adapted viruses dominate after only a few passages), viruses that have a high affinity for HS are attenuated for cattle (Sa-Carvalho *et al.*, 1997) and infection of cattle by an HS-binding strain gives rise to virulent, reverted viruses that have lost the ability to bind HS. This suggests that a high affinity for HS is a disadvantage in an animal, although field strains may make low-affinity interactions, enabling 'sampling' interactions to bring the virus into contact with cells and so increase integrin-mediated virus uptake. Alternatively, the ability to switch rapidly between high and low affinity for HS may be a determinant of tissue specificity and persistence (Fry *et al.*, 1999).

The selective pressure on field strains to adapt to cell culture is of practical concern to the vaccine industry. Field isolates seem to be very selective in their choice of integrin and grow very poorly in cell culture unless their required integrin is expressed. This may explain the switch to bind HS in type O viruses, which is achieved easily in cell culture by the substitution of arginine for histidine at position 56 of VP3. The ability of a single amino acid change to alter receptor-binding characteristics has been observed for other viruses and may be generally important in modulating pathogenicity. The effect of a single substitution may be enhanced by the number of potential binding sites on a virion (60 in this case). HS polymers have fully sulphated motifs [required for binding to FMDV O_1BFS (Fry *et al.*, 1999) and $A10_{61}$] at intervals of 50 Å and might wrap around the virion. The HS-binding site is located some 15 Å away from the RGD motif in the reduced conformation (although in this conformation it does not bind integrin) and the RGD-bearing VP1 GH loop is unaffected by heparin binding (Fry *et al.*, 1999). The two sites appear to function independently of each other and tissue culture-adapted strains can use either class of receptor.

In FMDVs, the integrin-binding site overlaps antigenic sites 1 and 5 and the HS-binding site overlaps antigenic site 4, resulting in a dilemma for the viruses in balancing receptor conservation and antigenic variation.

There are a vast number and variety of heparin-binding proteins, although as yet only a limited repertoire of atomic-resolution complex structures. Amongst these, the heparin-binding sites show no absolute dependency on specific sequences or protein folds and the extent to which the protein structure changes to accommodate the heparin varies considerably (Ganesh *et al.*, 2004; Mulloy & Linhardt, 2001). A trisaccharide motif seems to form a minimal binding unit, consistent with the helical structure of heparin, but the only generalization that can be made thus far is that all complexes use a mix of electrostatic and van der Waals interactions.

ACKNOWLEDGEMENTS

We particularly thank the disease security officers David Goodridge and Stuart Williams and the staff at the SRS for facilitating data collection. The project was supported by the BBSRC and MRC.

REFERENCES

Acharya, R., Fry, E., Stuart, D., Fox, G., Rowlands, D. & Brown, F. (1989). The three-dimensional structure of foot-and-mouth disease virus at 2·9 Å resolution. *Nature* **337**, 709–716.

Baranowski, E., Sevilla, N., Verdaguer, N., Ruiz-Jarabo, C. M., Beck, E. & Domingo, E. (1998). Multiple virulence determinants of foot-and-mouth disease virus in cell culture. *J Virol* **72**, 6362–6372.

Baranowski, E., Ruiz-Jarabo, C. M., Sevilla, N., Andreu, D., Beck, E. & Domingo, E. (2000). Cell recognition by foot-and-mouth disease virus that lacks the RGD integrin-binding motif: flexibility in aphthovirus receptor usage. *J Virol* **74**, 1641–1647.

Baxt, B., Vakharia, V., Moore, D. M., Franke, A. J. & Morgan, D. O. (1989). Analysis of neutralizing antigenic sites on the surface of type A_{12} foot-and-mouth disease virus. *J Virol* **63**, 2143–2151.

Berman, H. M., Westbrook, J., Feng, Z., Gilliland, G., Bhat, T. N., Weissig, H., Shindyalov, I. N. & Bourne, P. E. (2000). The Protein Data Bank. *Nucleic Acids Res* **28**, 235–242.

Bernard, K. A., Klimstra, W. B. & Johnston, R. E. (2000). Mutations in the E2 glycoprotein of Venezuelan equine encephalitis virus confer heparan sulfate interaction, low morbidity, and rapid clearance from blood of mice. *Virology* **276**, 93–103.

Bernfield, M., Götte, M., Park, P. W., Reizes, O., Fitzgerald, M. L., Lincecum, J. & Zako, M. (1999). Functions of cell surface heparan sulfate proteoglycans. *Annu Rev Biochem* **68**, 729–777.

Boothroyd, J. C., Harris, T. J. R., Rowlands, D. J. & Lowe, P. A. (1982). The nucleotide sequence of cDNA coding for the structural proteins of foot-and-mouth disease virus. *Gene* **17**, 153–161.

Brunger, A. T. (1992). XPLOR Version 3.1. New Haven, CT: Yale University Press.

Byrnes, A. P. & Griffin, D. E. (2000). Large-plaque mutants of Sindbis virus show reduced binding to heparan sulfate, heightened viremia, and slower clearance from the circulation. *J Virol* **74**, 644–651.

Cardin, A. D. & Weintraub, H. J. (1989). Molecular modeling of protein-glycosaminoglycan interactions. *Arteriosclerosis* **9**, 21–32.

Collaborative Computational Project, Number 4 (1994). The *CCP*4 suite: programs for protein crystallography. *Acta Crystallogr D Biol Crystallogr* **50**, 760–763.

Crowther, J. R., Farias, S., Carpenter, W. C. & Samuel, A. R. (1993). Identification of a fifth neutralizable site on type O foot-and-mouth disease virus following characterization of single and quintuple monoclonal antibody escape mutants. *J Gen Virol* **74**, 1547–1553.

Curry, S., Abu-Ghazaleh, R., Blakemore, W. & 7 other authors (1992). Crystallization and preliminary X-ray analysis of three serotypes of foot-and-mouth disease virus. *J Mol Biol* **228**, 1263–1268.

Curry, S., Fry, E., Blakemore, W. & 7 other authors (1996). Perturbations in the surface structure of A22 Iraq foot-and-mouth disease virus accompanying coupled changes in host cell specificity and antigenicity. *Structure* **4**, 135–145.

Escribano-Romero, E., Jimenez-Clavero, M. A., Gomes, P., García-Ranea, J. A. & Ley, V. (2004). Heparan sulphate mediates swine vesicular disease virus attachment to the host cell. *J Gen Virol* **85**, 653–663.

Esko, J. D., Weinke, J. L., Taylor, W. H., Ekborg, G., Rodén, L., Anantharamaiah, G. & Gawish, A. (1987). Inhibition of chondroitin and heparan sulfate biosynthesis in Chinese hamster ovary cell mutants defective in galactosyltransferase I. *J Biol Chem* **262**, 12189–12195.

Esnouf, R. M. (1997). An extensively modified version of MolScript that includes greatly enhanced coloring capabilities. *J Mol Graph Model* **15**, 132–134.

Esnouf, R. M. (1999). Further additions to *MolScript* version 1.4, including reading and contouring of electron-density maps. *Acta Crystallogr D Biol Crystallogr* **55**, 938–940.

Faham, S., Hileman, R. E., Fromm, J. R., Linhardt, R. J. & Rees, D. C. (1996). Heparin structure and interactions with basic fibroblast growth factor. *Science* **271**, 1116–1120.

Filman, D. J., Syed, R., Chow, M., Macadam, A. J., Minor, P. D. & Hogle, J. M. (1989). Structural factors that control conformational transitions and serotype specificity in type 3 poliovirus. *EMBO J* **8**, 1567–1579.

Fox, G., Parry, N. R., Barnett, P. V., McGinn, B., Rowlands, D. J. & Brown, F. (1989). The cell attachment site on foot-and-mouth disease virus includes the amino acid sequence RGD (arginine-glycine-aspartic acid). *J Gen Virol* **70**, 625–637.

Fry, E., Acharya, R. & Stuart, D. (1993). Methods used in the structure determination of foot-and-mouth disease virus. *Acta Crystallogr A* **49**, 45–55.

Fry, E. E., Lea, S. M., Jackson, T. & 7 other authors (1999). The structure and function of a foot-and-mouth disease virus–oligosaccharide receptor complex. *EMBO J* **18**, 543–554.

Ganesh, V. K., Smith, S. A., Kotwal, G. J. & Murthy, K. H. M. (2004). Structure of vaccinia complement protein in complex with heparin and potential implications for complement regulation. *Proc Natl Acad Sci U S A* **101**, 8924–8929.

Goodfellow, I. G., Sioofy, A. B., Powell, R. M. & Evans, D. J. (2001). Echoviruses bind heparan sulfate at the cell surface. *J Virol* **75**, 4918–4921.

Harlos, K. (1992). Micro-bridges for sitting-drop crystallizations. *J Appl Crystallogr* **25**, 536–538.

Jackson, T., Ellard, F. M., Abu Ghazaleh, R., Brookes, S. M., Blakemore, W. E., Corteyn, A. H., Stuart, D. I., Newman, J. W. I. & King, A. M. Q. (1996). Efficient infection of cells in culture by type O foot-and-mouth disease virus requires binding to cell surface heparan sulfate. *J Virol* **70**, 5282–5287.

Jackson, T., Sharma, A., Abu Ghazaleh, R., Blakemore, W. E., Ellard, F. M., Simmons, D. L., Newman, J. W. I., Stuart, D. I. & King, A. M. Q. (1997). Arginine-glycine-aspartic acid-specific binding by foot-and-mouth disease viruses to the purified integrin $\alpha v\beta 3$ in vitro. *J Virol* **71**, 8357–8361.

Jackson, T., Sheppard, D., Denyer, M., Blakemore, W. & King, A. M. Q. (2000). The epithelial integrin $\alpha v\beta 6$ is a receptor for foot-and-mouth disease virus. *J Virol* **74**, 4949–4956.

Jackson, T., Mould, A. P., Sheppard, D. & King, A. M. Q. (2002). Integrin $\alpha v\beta 1$ is a receptor for foot-and-mouth disease virus. *J Virol* **76**, 935–941.

Jackson, T., King, A. M. Q., Stuart, D. I. & Fry, E. (2003). Structure and receptor binding. *Virus Res* **91**, 33–46.

Jackson, T., Clark, S., Berryman, S., Burman, A., Cambier, S., Mu, D., Nishimura, S. & King, A. M. Q. (2004). Integrin $\alpha v\beta 8$ functions as a receptor for foot-and-mouth disease virus: role of the β-chain cytodomain in integrin-mediated infection. *J Virol* **78**, 4533–4540.

Jones, T. A. (1985). Interactive computer graphics: FRODO. *Methods Enzymol* **115**, 157–171.

Kim, S. S., Smith, T. J., Chapman, M. S., Rossmann, M. C., Pevear, D. C., Dutko, F. J., Felock, P. J., Diana, G. D. & McKinlay, M. A. (1989). Crystal structure of human rhinovirus serotype 1A (HRV1A). *J Mol Biol* **210**, 91–111.

Kitson, J. D. A., McCahon, D. & Belsham, G. J. (1990). Sequence analysis of monoclonal antibody resistant mutants of type O foot and mouth disease virus: evidence for the involvement of the three surface exposed capsid proteins in four antigenic sites. *Virology* **179**, 26–34.

Klimstra, W. B., Ryman, K. D. & Johnston, R. E. (1998). Adaptation of Sindbis virus to BHK cells selects for use of heparan sulfate as an attachment receptor. *J Virol* **72**, 7357–7366.

Kraulis, P. J. (1991). *MOLSCRIPT*: a program to produce both detailed and schematic plots of protein structures. *J Appl Crystallogr* **24**, 946–950.

Lea, S., Hernandez, J., Blakemore, W. & 9 other authors (1994). The structure and antigenicity of a type C foot-and-mouth disease virus. *Structure* **2**, 123–139.

Lea, S., Abu-Ghazaleh, R., Blakemore, W. & 7 other authors (1995). Structural comparison of two strains of foot-and-mouth disease virus subtype O_1 and a laboratory antigenic variant, G67. *Structure* **3**, 571–580.

Lee, E. & Lobigs, M. (2002). Mechanism of virulence attenuation of glycosaminoglycan-binding variants of Japanese encephalitis virus and Murray Valley encephalitis virus. *J Virol* **76**, 4901–4911.

Logan, D., Abu-Ghazaleh, R., Blakemore, W. & 10 other authors (1993). Structure of a major immunogenic site on foot-and-mouth disease virus. *Nature* **362**, 566–568.

Mandl, C. W., Kroschewski, H., Allison, S. L., Kofler, R., Holzmann, H., Meixner, T. & Heinz, F. X. (2001). Adaptation of tick-borne encephalitis virus to BHK-21 cells results in the formation of multiple heparan sulfate binding sites in the envelope protein and attenuation in vivo. *J Virol* **75**, 5627–5637.

Mason, P. W., Baxt, B., Brown, F., Harber, J., Murdin, A. & Wimmer, E. (1993). Antibody-complexed foot-and-mouth disease virus, but not poliovirus, can infect normally insusceptible cells via the Fc receptor. *Virology* **192**, 568–577.

Merritt, E. A. & Murphy, M. E. P. (1994). *Raster3D* version 2.0. A program for photorealistic molecular graphics. *Acta Crystallogr D Biol Crystallogr* **50**, 869–873.

Mulloy, B. & Linhardt, R. J. (2001). Order out of complexity – protein structures that interact with heparin. *Curr Opin Struct Biol* **11**, 623–628.

Neff, S., Sá-Carvalho, D., Rieder, E., Mason, P. W., Blystone, S. D., Brown, E. J. & Baxt, B. (1998). Foot-and-mouth disease virus virulent for cattle utilizes the integrin $\alpha_v\beta_3$ as its receptor. *J Virol* **72**, 3587–3594.

Nicholls, A., Sharp, K. A. & Honig, B. (1991). Protein folding and association: insights from the interfacial and thermodynamic properties of hydrocarbons. *Proteins* **11**, 281–296.

Otwinoski, Z. (1993). Oscillation data reduction program. In *Proceedings of the CCP4 Study Weekend: Data Collection and Processing*, 29–30 January, 1993, pp. 56–62. Warrington, UK: Daresbury Laboratory, SERC.

Parry, N., Fox, G., Rowlands, D., Brown, F., Fry, E., Acharya, R., Logan, D. & Stuart, D. (1990). Structural and serological evidence for a novel mechanism of antigenic variation in foot-and-mouth disease virus. *Nature* **347**, 569–572.

Reddi, H. V., Kumar, A. S. M., Kung, A. Y., Kallio, P. D., Schlitt, B. P. & Lipton, H. L. (2004). Heparan sulfate-independent infection attenuates high-neurovirulence GDVII virus-induced encephalitis. *J Virol* **78**, 8909–8916.

Sa-Carvalho, D., Rieder, E., Baxt, B., Rodarte, R., Tanuri, A. & Mason, P. W. (1997). Tissue culture adaptation of foot-and-mouth disease virus selects viruses that bind to heparin and are attenuated in cattle. *J Virol* **71**, 5115–5123.

Spillmann, D. (2001). Heparan sulfate: anchor for viral intruders? *Biochimie* **83**, 811–817.

Stehle, T., Yan, Y., Benjamin, T. L. & Harrison, S. C. (1994). Structure of murine polyomavirus complexed with an oligosaccharide receptor fragment. *Nature* **369**, 160–163.

Strohmaier, K., Franze, R. & Adam, K.-H. (1982). Location and characterization of the antigenic portion of the FMDV immunizing protein. *J Gen Virol* **59**, 295–306.

Stuart, D. I., Levine, M., Muirhead, H. & Stammers, D. K. (1979). Crystal structure of cat muscle pyruvate kinase at a resolution of 2·6 Å. *J Mol Biol* **134**, 109–142.

Thomas, A. A. M., Woortmeijer, R. J., Puijk, W. & Barteling, S. J. (1988). Antigenic sites on foot-and-mouth disease virus type A10. *J Virol* **62**, 2782–2789.

Verdaguer, N., Mateu, M. G., Andreu, D., Giralt, E., Domingo, E. & Fita, I. (1995). Structure of the major antigenic loop of foot-and-mouth disease virus complexed with a neutralizing antibody: direct involvement of the Arg-Gly-Asp motif in the interaction. *EMBO J* **14**, 1690–1696.

Verdaguer, N., Fita, I., Domingo, E. & Mateu, M. G. (1997). Efficient neutralization of foot-and-mouth disease virus by monovalent antibody binding. *J Virol* **71**, 9813–9816.

Wallace, A. C., Laskowski, R. A. & Thornton, J. M. (1995). LIGPLOT: a program to generate schematic diagrams of protein–ligand interactions. *Protein Eng* **8**, 127–134.

Zautner, A. E., Körner, U., Henke, A., Badorff, C. & Schmidtke, M. (2003). Heparan sulfates and coxsackievirus-adenovirus receptor: each one mediates coxsackievirus B3 PD infection. *J Virol* **77**, 10071–10077.

Zhao, Q., Pacheco, J. M. & Mason, P. W. (2003). Evaluation of genetically engineered derivatives of a Chinese strain of foot-and-mouth disease virus reveals a novel cell-binding site which functions in cell culture and in animals. *J Virol* **77**, 3269–3280.